Journal of Molecular Structure 1232 (2021) 130032

Contents lists available at ScienceDirect

Journal of Molecular Structure

journal homepage: www.elsevier.com/locate/molstr

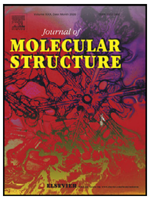

Synthesis of coordination polymers of cobalt *meso*-pyridylporphyrins and its oxygen reduction properties

Neha Saran, Tincy Lis Thomas, Purushothaman Bhavana*

Birla Institute of Technology and Science (BITS), Pilani, K. K. Birla Goa Campus, Goa, 403726, India

ARTICLE INFO

Article history:
Received 16 November 2020
Revised 16 January 2021
Accepted 27 January 2021
Available online 31 January 2021

Keywords:
Pyridylporphyrins
Coordination polymer
O_2 reduction
Pyrolysis
Metalation
RDE

ABSTRACT

The present work sheds light on the role of coordinating side groups on the porphine ring in deciding the extent of the metalation reaction as well as the formation of coordination polymers of porphyrin. Electrocatalytic activity of coordination polymers of isomers of pyridylporphyrins has been investigated after pyrolysing them at different temperatures. The pyrolysed materials were characterized by XRD, XPS, SEM, TEM and BET techniques. The electrocatalytic behaviour of the sample were investigated by modifying the glassy carbon electrode with the sample (in both normal and pyrolysed form). The electrode modified using the pyrolysed sample of polymerized pyridylporphyrin at 800 °C acted as a good electrocatalyst for the reduction of dioxygen. The studies on kinetics of oxygen reduction using rotating disk electrode shows the reduction through 2-electron pathway forming H_2O_2 in alkaline medium.

1. Introduction

Porphyrins with aromatic groups at the *meso* position are macrocyclic molecules with aromatic π- system that has different types of sites available for further functionalization. It forms complexes with a variety of metal ions of varying sizes, oxidation number and coordination properties. Depending on the above mentioned properties, it forms planar [1], siting-a-top [2] or sandwich complexes [3]. Based on its coordination properties, the metal centre in planar porphyrin can be tetra (with only porphyrin ligand) or, penta or hexa (with porphyrin and, one or two axial ligands respectively) coordinated. Though the coordination chemistry of the centre part of this class of molecules is extensively investigated, the same at the periphery of the molecule has received less attention [4,5].

In *meso*-tetraphenylporphyrins, the four phenyl groups present at the *meso* position of the molecule are known to be oriented perpendicular to the centre part of the molecule [6,7]. These groups do not influence the coordination chemistry of the molecule to a great extent. Other than phenyl groups, porphyrinic molecules with alkyl and other aromatic (homo- or hetero-) groups are well reported. Depending on the size and shape of the *meso*-groups and also on the heteroatom present on it, the self-assembling properties/supramolecular architecture are decided [8].

One of the special classes of heteroaromatic porphyrins is *meso*-pyridylporphyrins. In this, the substituents at the *meso*-positions have nearly same size as that of phenyl in the tetraphenylporphyrin [compared to the other side groups of bigger (naphthyl, anthracenyl, quinolinyl etc.) or smaller (imidazolyl, thienyl etc.) size generally seen in synthetic porphyrins]. The presence of nitrogen on the side group makes this porphyrin very interesting in its coordination behaviour (as in imidazolylporphyrins). Pyridylporphyrins are known for sensing [9–11] and catalytic [12,13] activities. They are known for their tendency to form coordination polymers with different metal ions [14–18]. Their hydrogen bonding properties also have been reported [19]. Pyridine molecules are known for the coordination properties [20]. One of the nonameric porphyrin reported in literature has a tetrapyridylporphyrin as one of the constituents [21]. The metalation reactions of pyridylporphyrins are generally carried out using the solvent dimethylformamide (DMF) under normal metalation condition [22–24], hydrothermally [16] or in presence of acid or organic base [12,25]. The compounds derived from these reactions are further studied in DMF for their applications.

In the research on fuel cells, the cathodic process attained more attention due to the slow kinetics of dioxygen reduction on conventional electrodes. The use of platinum as the electrode, though the most effective found till date, is limited in application due to its high cost and scarcity. One of the aims of research on fuel cells is to replace the Pt electrode with an economically viable elec-

---

* Corresponding author at: Department of Chemistry, Birla Institute of Technology and Science (BITS), Pilani, K. K. Birla Goa Campus, Zuarinagar, Goa, 403 726, India.

E-mail addresses: tincy@goa.bits-pilani.ac.in (T.L. Thomas), pbhavana@goa.bits-pilani.ac.in (P. Bhavana).

https://doi.org/10.1016/j.molstruc.2021.130032
0022-2860/

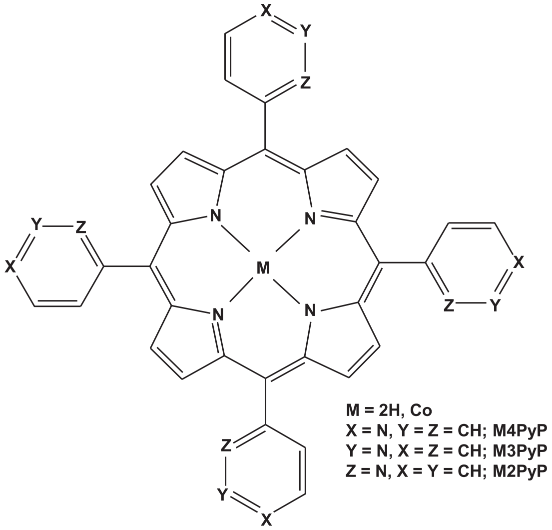

Fig. 1. Molecular structure of the compounds used for the study.

trode. In this scenario, non-noble metal catalysts have gained importance in oxygen reduction reactions (ORR). Extensive research has been carried out using porphyrin as catalyst (electrode modifying agent) in the electrochemical reduction of dioxygen. Porphyrins, either used as such [26,27] or used in the form of hybrid [28] or composite [29] with other suitable materials, are investigated as the electrode modifying agents. The electrochemical dioxygen reduction properties of pyridylporphyrins in its water soluble form is widely studied [22,30–38]. Water insoluble pyridylporphyrins are relatively less explored for the same application [39–44].

In the present work, metalation of pyridylporphyrin using cobalt acetate was carried out using the commonly used chloroform – methanol solvent system. The primary aim of the study was to investigate the coordination behaviour of the *meso*-groups of different isomers of porphyrin. So we have selected pyridylporphyrins as its coordination chemistry depends on the position of the pyridinic-N. The study also intends to find out a method of increasing the cobalt content in the synthesized (metalated) product for ORR. The prepared compounds were pyrolysed under different temperature and their electrocatalytic oxygen reduction properties were investigated. Fig. 1 shows the molecular structure of the porphyrins used for the present investigation and the abbreviations.

2. Experimental

2.1. Materials and methods

Pyrrole, 2-pyridinecarboxaldehyde, 3-pyridinecarboxaldehyde, 4-pyridinecarboxaldehyde cobalt(II) acetate tetrahydrate and Nafion® 117 solution (~ 5% in a mixture of lower aliphatic alcohols and water) were purchased from Sigma–Aldrich. Chloroform, methanol, propionic acid, acetic anhydride, potassium hydroxide and DMF were purchased from SD Fine Chemicals, India. Neutral alumina was obtained from Fischer scientific. Milli-Q water was used for preparation of all the electrolyte solutions.

Optical absorption spectra were recorded on a JASCO V-570 model UV/VIS/NIR spectrophotometer using quartz cells of 1 cm path length. ^{1}H NMR spectra were recorded on a DRX-500 spectrometer in deuterated chloroform using tetramethylsilane as the internal standard. Mass spectrum was recorded on a Agilent Technology Model 6460 Triple Quadrupole LC/MS consisting 1290 infinity II Binary Pump, auto sampler and Diode array detector (ESI).

The metal content in each catalyst was analysed by inductively coupled plasma-atomic emission spectrometry (ICP-AES, ARCOS Simultaneous ICP Spectrometer SPECTRO Analytical Instruments GmbH, Germany). A FEG 250 (Quanta) scanning electron microscope (SEM) was used to investigate the morphology of catalyst. Transmission electron microscopy (TEM) images were recorded on Tecnai G2, F30 transmission electron microscope at an acceleration voltage of 300 kV. Powder X-ray diffraction patterns (XRD) were recorded on Bruker D8 Advance diffractometer. X-ray photoelectron spectra (XPS) of the synthesized catalysts were recorded on a PHI 5000 Versa Prob II (FEI Inc.) spectrometer using Al K_α radiation (1486.6 eV). A Microtrac BEL Corp mini-II surface area analyser was used to measure the surface area, pore size distribution and N_2 physisorption isotherms of the materials at 77 K. Degassing was carried out in vacuum at 100 °C for 2 h on the synthesized materials before starting the sorption measurements.

The linear sweep voltammetry experiments and the experiments using rotating disc electrode (RDE-2, Bioanalytical systems) were carried out using BASi EPSILON model electrochemical work station. Modified glassy carbon electrode, Ag/AgCl electrode and spiral platinum wire were used, respectively, as working, reference and auxiliary electrodes. All measurements related to reduction of dioxygen were performed in 0.1 M KOH solution purged with dioxygen for 30 min (unless otherwise mentioned).

2.2. Synthesis

2.2.1. Synthesis of free base meso-tetrapyridylporphyrin (H_2APyP, $A = 2, 3$ or 4)

The free base porphyrins were synthesized by following the general procedure for the synthesis of free base porphyrins by Adler *et al.* with modifications in it, using the respective aldehydes [45,46]. Typically, to 120 mL of propionic acid under refluxing conditions, 2.7 mL (29.8 mmol) of pyridine-4-carboxaldehyde followed by 2 mL (29.8 mmol) of pyrrole were added. This was followed by the addition of 4.8 mL of acetic anhydride in the reaction mixture. Refluxing the reaction mixture was continued for 30 min. At the end of this period, the crude product was collected by distillation under reduced pressure. The free base porphyrin was purified by column chromatography using neutral alumina as the packing material and chloroform - methanol as the eluting mixture. The product obtained was purple in colour. It was characterized by UV visible, ^{1}H NMR and mass spectroscopic techniques.

The yield of the product was 650 mg (14.59%), 810 mg (18.2%) and 950 mg (21.3%) for $H_2$2PyP, $H_2$3PyP and $H_2$4PyP, respectively.

2.2.2. Synthesis (of polymeric form) of cobalt containing meso-tetrapyridylporphyrin (p-CoAPyP, $A = 2, 3$ or 4). Insertion of cobalt ion in free base porphyrin was carried out using two different equivalents of cobalt(II) acetate tetrahydrate.

(a) Using five equivalence of cobalt acetate tetrahydrate

To 50 mg (0.08 mM) of $H_2$4PyP in 20 mL of chloroform, 100.64 mg (0.4 mM) of cobalt(II) acetate tetrahydrate in 6 mL of methanol was added and refluxed for 4 h. The precipitate formed during the course of the reaction was collected by centrifugation. The crude product obtained was treated with water repeatedly (till the washing did not show the presence of cobalt acetate by UV visible spectroscopy). The solid was dried under vacuum at 100 °C for 12 h. The yield of the product was 51.7 mg.

(a) Using one equivalence of cobalt acetate tetrahydrate

Same procedure given above was followed in this reaction (using 50 mg of porphyrin and 20.12 mg of cobalt acetate tetrahydrate). The yield of the product (precipitate after treating with water and drying) was 22.9 mg.

Same procedure (**a** and **b**) was followed for the metalation of $H_2$3PyP and $H_2$2PyP and the yield obtained are as follows.
Procedure **a**: 33.5 mg for $H_2$3PyP and 28.0 mg for $H_2$2PyP
Procedure **b**: 11.8 mg for $H_2$3PyP and 5.1 mg for $H_2$2PyP

2.3. Preparation of catalyst

Electrocatalyst was prepared by pyrolysing the porphyrin using alumina crucible in a tubular furnace. The *p*-Co4PyP sample was heated from room temperature to 400 °C (*p*-Co4PyP-400), 600 °C (*p*-Co4PyP-600) and 800 °C (*p*-Co4PyP-800) separately with a heating rate of 3 °C/min under nitrogen atmosphere. Similar pyrolysis treatment was done for *p*-Co3PyP and the naming was done accordingly (*p*-Co3PyP-400, *p*-Co3PyP-600 and *p*-Co3PyP-800).

2.4. Electrode preparation and electrochemical measurements

All electrochemical studies were carried out by linear sweep voltammetry (using rotating disk electrode (RDE)) technique. For modifying the electrode 1.0 mg catalyst was suspended in 470 μL of ethanol and 500 μL of water containing 30 μL of Nafion®. This solution was sonicated for two hours to form stable suspension. 2.5μL of the solution was dropped on glassy carbon electrode (GCE) and dried in air. Scanning was done in the potential range 0.0 V to −1.2 V at a scan speed of 10 mV/s at different rotating speed ranging from 100 to 2600 rpm in the oxygen saturated solution of 0.1 M KOH.

Analysis of the results obtained using RDE measurements was done using Koutecky-Levich (K-L) equation [47]

$$1/J = 1/\left(B\omega^{1/2}\right) + J_k$$

$$B = 0.2nFC_{O2}\left(D_{O2}\right)^{2/3}\upsilon^{-1/6}$$

In this equation, J is the measured current density, J_k is the kinetic current density of the oxygen reduction reaction, n is the number of electrons, F is the Faraday constant, D is the diffusion coefficient of O_2 ($D_{O2} = 1.9 \times 10^{-5}$ cm^2s^{-1}), υ is the kinetic viscosity of the electrolyte ($\upsilon = 0.01$ cm^2s^{-1}), ω is the rate of rotation of the electrode and C_{O2} is the bulk concentration of O_2 ($C_{O2} = 1.2 \times 10^{-6}$ $molcm^{-3}$) in 0.1 M aqueous KOH. Slope of K-L (J^{-1} vs $\omega^{-1/2}$) plot gives the value of B.

3. Results and discussion

3.1. Synthesis

The incorporation of cobalt ion at the core of H_2APyP (**A = 2, 3 or 4**) using cobalt acetate tetrahydrate was carried out in chloroform – methanol solvent system. Metal insertion reactions were carried out with different ratio of free base porphyrin to cobalt acetate (1:5 and 1:1). The addition of 5 equivalents of cobalt acetate has resulted in the nearly complete precipitation of the product in the case of $H_2$4PyP. The supernatant liquid in the reaction mixture turned almost colourless at the end of the reaction (case **a**). The UV visible spectrum indicated the presence of trace amount of freebase porphyrin in the mother liquor. After refluxing for 4 h, the product was washed repeatedly with water (till the washings showed the absence of cobalt acetate as evidenced by UV visible spectroscopy). In all the commonly used organic solvents (except DMF, in which the compound dissolved to a great extent over a period of time), the product was insoluble. UV visible spectrum of the product recorded in DMF showed the spectrum corresponding to metalated porphyrin suggesting the incorporation of cobalt metal ion at the centre of the porphyrin (one Soret and two Q bands with second Q band appearing as a shoulder, Fig. 2). Similar reaction carried out with only one equivalent of cobalt acetate has resulted in relatively less amount of precipitate (22.9 mg) and an intensely coloured supernatant liquid (which showed the presence of free base porphyrin; indicating relatively higher amount of unreacted free base (case **b**)). This has indicated that the incorporation of cobalt at the core of the porphyrin is incomplete in case **b**. The precipitate formed in both reactions showed similar solubility characteristics.

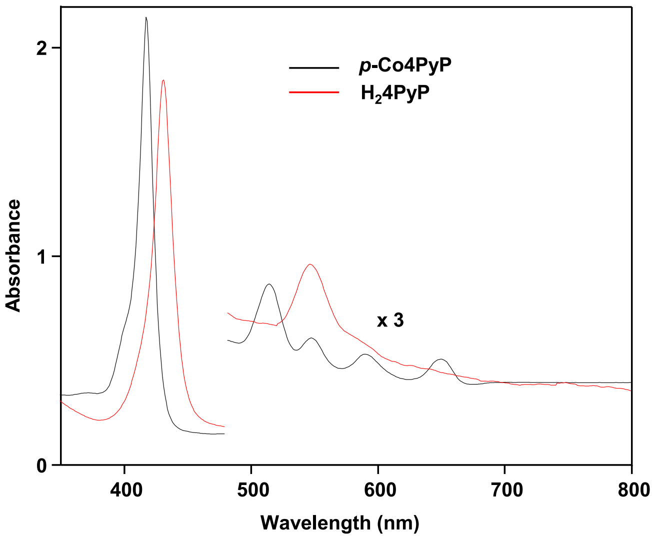

Fig. 2. UV visible absorption spectrum of $H_2$4PyP and p-Co4PyP recorded in DMF.

Similar metalation procedure was followed for 2- and 3-pyridylporphyrins. In the case of $H_2$2PyP, the amount of metalated product (precipitate) obtained was very less (from 50 mg of the starting material, 11.8 mg in case **a** and 5.1 mg in case **b**). The supernatant liquid contain large amount of free base porphyrin even after refluxing for extended duration (8 h). Similar reaction of $H_2$3PyP has resulted in the product to unreacted starting material ratio in between that of $H_2$2PyP and $H_2$4PyP.

The dependence on the quantity of precipitate (the product) to the amount of cobalt acetate added and the solubility characteristics have led to the conclusion that the pyridyl group of the porphyrins is acting as ligand to interact with cobalt metal ion at the periphery of the porphyrin (along with the insertion at the centre of the molecule as evidenced from UV visible spectra). The ligation has resulted in a polymerised structure. As the coordination is easy due to the favored symmetric structure of the 4-pyridylporphyrin, the amount of polymerized product formed is maximum (supernatent liquid showed presence of only small amount of freebase porphyrin in case **a**). This is supported by the relatively less amount of the precipitate formed in the cases of $H_2$3PyP and $H_2$2PyP. Among $H_2$3PyP and $H_2$2PyP, the amount of metalated (polymerized) product is more for $H_2$3PyP. This can be attributed to the less steric constraints present in $H_2$3PyP compared to that in $H_2$2PyP in forming a coordinate bond through the pyridyl-N to the cobalt metal ion (Fig. 3). Since the amount of precipitate formed in $H_2$2PyP is very less, further investigation was not carried out with this porphyrin.

Synthesis of cobalt complex of 4-pyridylporphyrin is reported in literature [22–24] with DMF or others [12,25] as the solvent for metal insertion reaction. In any of the report, formation of precipitate during the metalation reaction is not mentioned. In order to confirm the polymerized structure of the metalated product under the reaction condition of the present work, ICP-AES of metalated products of both $H_2$4PyP and $H_2$3PyP (named *p*-Co4PyP and *p*-Co3PyP, respectively) was carried out. The percentage of cobalt is 13.01% and 12%, respectively, for *p*-Co4PyP and *p*-Co3PyP. If it was

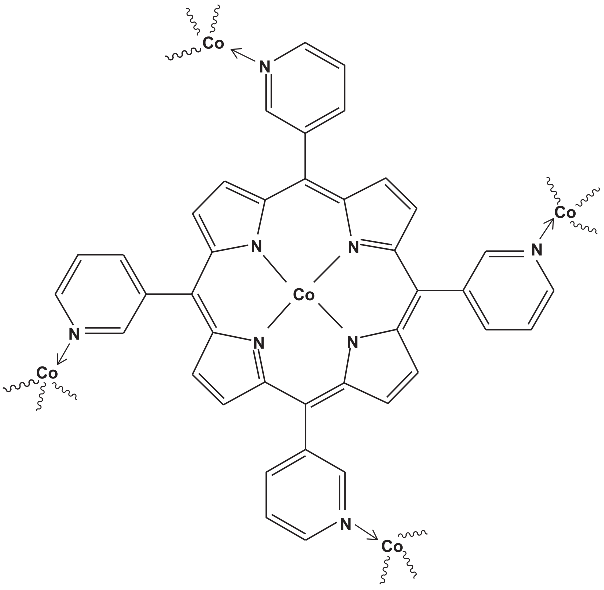

Fig. 3. Incorporation of cobalt metal ion in *meso*-3-pyridylporphyrin.

a monomeric metalated product, the percentage of cobalt present in the sample should have been 8.55%. So the obtained ICP-AES results (i.e., the presence of more than one cobalt ion per porphyrin ring) confirm the formation of coordination polymers of pyridylporphyrins in presence of cobalt metal ion carrier in the solvent system chloroform – methanol. The relatively lesser amount of cobalt in *p*-Co3PyP is attributed to the unfavourable geometry of 3-pyridyl group of porphyrin in interacting with the cobalt metal ion through N of the pyridyl group. In the cobalt insertion reactions reported in literature using DMF as the solvent, no coordination with cobalt by the pyridyl group at the periphery is reported to the best of our knowledge. In the reported crystal structures of Co4PyP and Co3PyP, pyridyl group of one molecule appeared as an axial ligand on cobalt of another molecule [5,8,16]. This axial coordination leads to the stoichiometry of 1:1 for cobalt ion to porphyrin ligand in these reported cases.

The synthesized porphyrin *p*-Co4PyP dispersed (1 mg in 1 mL) in water:ethanol (1:1) was used to modify the surface of the glassy carbon electrode by drop-casting (using nafion as the binding agent). This modified electrode was used for the dioxygen reduction in alkaline medium (0.1 M KOH). Fig. 4 shows the reduction of dioxygen using modified electrode. *p*-Co3PyP also showed a similar activity, but to a lesser extent. The current generated was less in both the cases, though the onset potential was promising. In order to increase the activity, these cobalt containing coordination polymers were pyrolysed under different temperature and investigated as GCE modifying agent. Pyrolysis of the metalloorganic compounds is known for its increased activity towards dioxygen reduction [48].

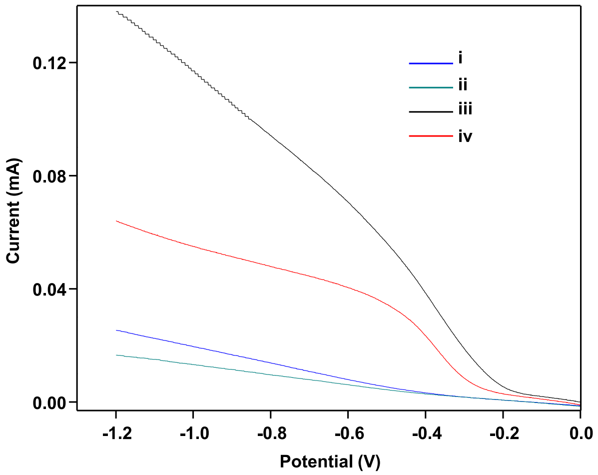

Fig. 4. Linear sweep voltammogram of (i) *p*-Co4PyP and (ii) *p*-Co3PyP under nitrogen; (iii) *p*-Co4PyP and (iv) *p*-Co3PyP under oxygen (all in 0.1 M KOH, 2600 rpm).

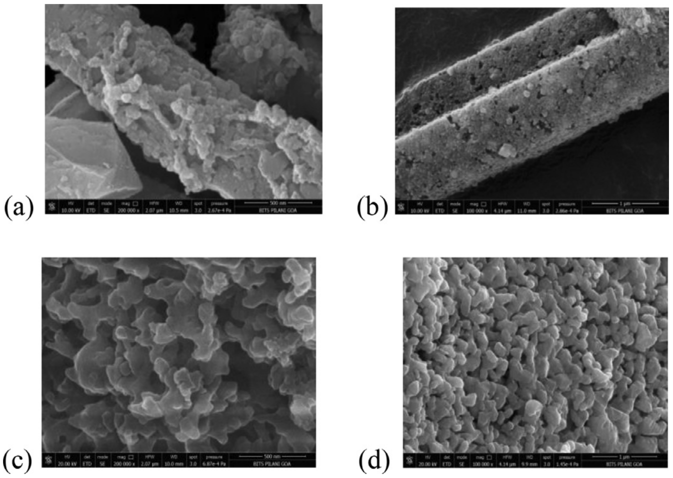

Fig. 5. SEM images (with scale bar given in figure) of (a) *p*-Co4PyP (500 nm), (b) *p*-Co4PyP-800 (1 μm), (c) *p*-Co3PyP (500 nm) and (d) *p*-Co3PyP-800 (1 μm).

3.2. Characterisation of the pyrolysed samples

3.2.1. Scanning electron microscopy (SEM)

SEM image of *p*-Co4PyP-800 showed a ribbon-like morphology with a length in the range 3.68 μm to 5.8 μm and width 375 nm to 500 nm. It has a highly porous structure (Fig. 5a and b). Similar morphology on pyrolysed porphyrins is reported for cobalt porphyrin conjugated polymers [49]. *p*-Co3PyP-800 showed small granular structure (Fig. 5c and d) [53]. SEM images of *p*-Co4PyP-600, *p*-Co4PyP-400, *p*-Co3PyP-600 and *p*-Co3PyP-400 are given in supplementary information (Figure S1). Compared to that of the unpyrolysed samples, the surface is smooth for the pyrolysed sample in all the cases indicating the formation of ordered carbonaceous matrix on heating.

3.2.2. Transmission electron microscopy (TEM & HRTEM)

Cobalt nanoparticles are found to be embedded in the matrix (Fig. 6a and b) [49] in the TEM images of *p*-Co4PyP-800. High resolution TEM images of *p*-Co4PyP-800 and *p*-Co3PyP-800 (Fig. 6c-f) and the XRD pattern (discussed below) indicate that the cobalt nanoparticles with a highly crystalline structure are encapsulated within graphitic carbon matrix

3.2.3. Powder X-ray diffraction analysis (XRD)

The XRD patterns of pyrolysed samples of both *p*-Co4PyP and *p*-Co3PyP at different temperatures are shown in Fig. 7. A very broad peak at 25° was observed in all the pyrolysed samples, which is assigned to the diffraction of carbon (002). The diffraction at 44° in the XRD pattern of all samples is attributed to cobalt (111) plane (PDF#89–4307). The sharpness of the diffraction peaks increased with temperature. The peak corresponding to cobalt (200) plane also appears on pyrolysis. These results indicate the formation of metallic Co during pyrolysis of the porphyrinic polymer. The material shows a weak diffraction feature of metallic Co (111) after heat treatment at 400 °C. On heat treatment at 600 °C and 800 °C both

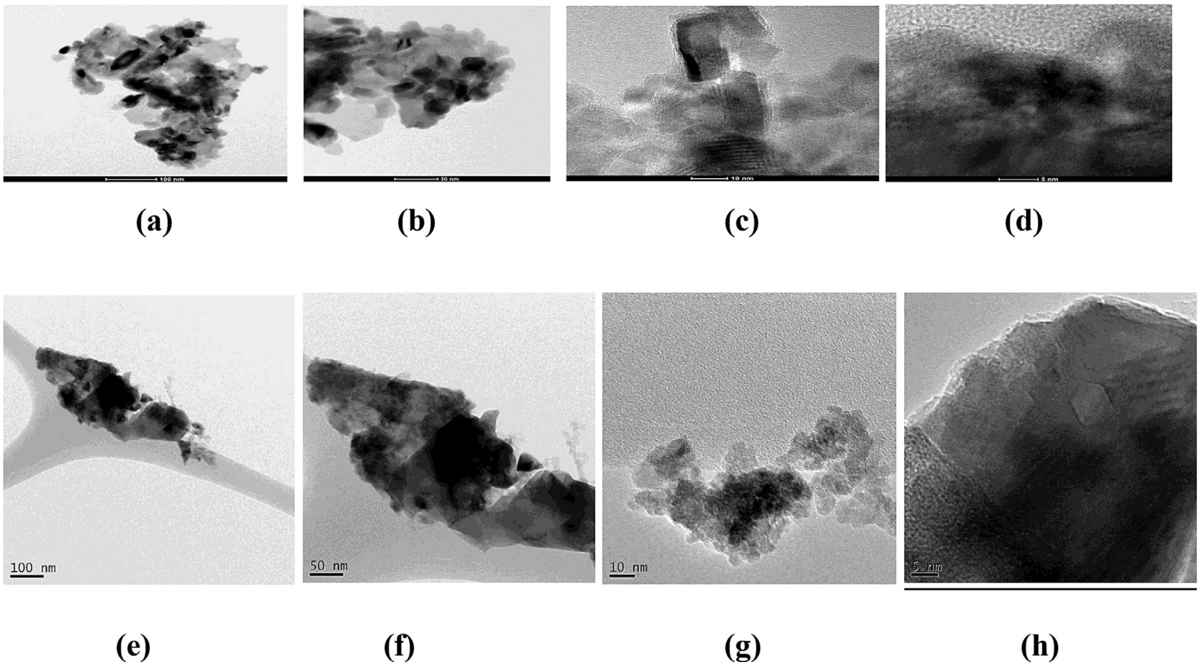

Fig. 6. TEM (a,b) and high-resolution TEM (c,d) images of the *p*-Co4PyP-800 and high-resolution TEM images of *p*-Co3PyP-800 (e-h).

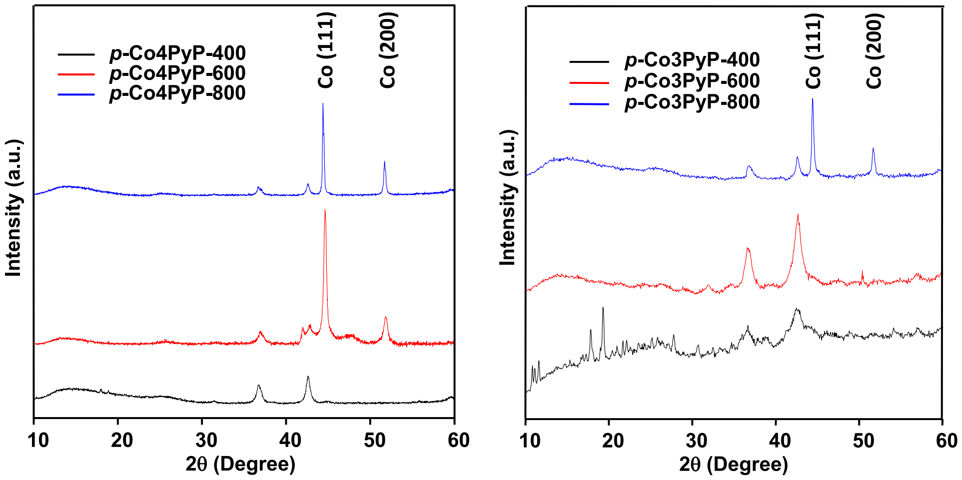

Fig. 7. Powder X-ray diffraction patterns of *p*-Co4PyP and *p*-Co3PyP pyrolysed at different temperatures.

metallic Co (111) and Co (200) peaks appear which indicates that the catalyst is transformed to a composite of cobalt and carbon on pyrolysis [50]. Also, with the increase in heating temperature, the diffraction peaks becomes sharper, indicating the increase in crystallanity of cobalt.

3.2.4. X-ray photoelectron spectroscopy (XPS)

XPS results showed the presence of peaks corresponding to C 1 s, N 1 s (weak), O 1 s and Co 2p in the samples of *p*-CoAPyP, *p*-CoAPyP-400, *p*-CoAPyP-600 and *p*-CoAPyP-800 ($A = 3$ or 4). The percentage of surface Co are 4.14 and 3.75 at%, respectively, for *p*-Co4PyP-800 and *p*-Co3PyP-800 (Table 1). This percentage content is found to be higher than that reported previously for 4-pyridylporphyrin (synthesized and studied differently). In the reported case, the atomic percentage of cobalt is 0.6 [24]. But the nitrogen content in this case is 6.8% which is higher than that for the samples of present study. In the reported work, authors have claimed that the species responsible for the electrocatalytic activity (ORR) is CoN_x centre even after pyrolysis [51]. However, in the present work, the nitrogen content is very less (2.36 atomic% for *p*-Co4PyP-800 and 0.59 atomic% for *p*-Co3PyP-800). The less amount

Table 1
Surface composition of different samples evaluated from the XPS analysis.

Sample	C(at%)	N(at%)	O(at%)	Co(at%)
p-Co4PyP	64.73	9.00	14.28	3.99
p-Co4PyP-400	69.60	8.45	11.98	1.45
p-Co4PyP-600	64.69	9.21	18.20	2.50
p-Co4PyP-800	65.92	2.36	19.79	4.14
p-Co3PyP	71.48	9.26	10.76	0.59
p-Co3PyP-400	70.12	8.45	7.88	0.67
p-Co3PyP-600	63.71	8.96	15.55	2.63
p-Co3PyP-800	64.06	0.59	23.64	3.75

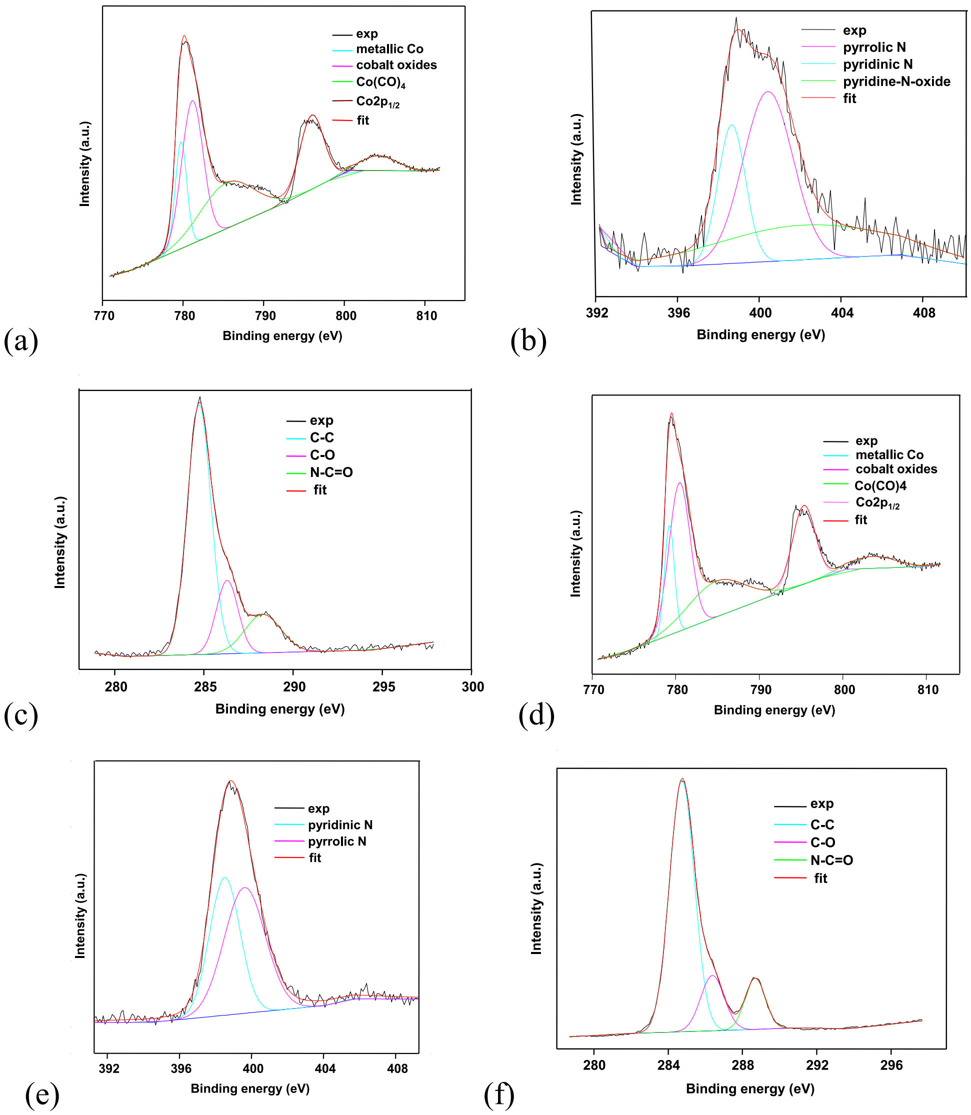

Fig. 8. XPS spectra of *p*-Co4PyP-800 catalyst: (a) Co 2p (b) N 1 s (c) C 1 s and of *p*-Co3PyP-800 catalyst: (d) Co 2p (e) N 1 s (f) C 1 s.

of nitrogen indicates that CoN_x centre is not being the active centre in this case.

In the article reported on the oxygen reduction activity of Co4PyP synthesized using DMF as the solvent [24] also it is given that CoN_4 centre is the cause for its ORR activity. But in the XPS investigation of the present work, we cannot see any peak corresponding to Co-N bond. Instead peak corresponding to Co nanoparticle is seen (discussed below). So Co metallic nanoparticle is expected to have a contribution in the ORR activity (Fig. 8). XRD also supported the presence of Co nanoparticle. From deconvoluted spectrum of *p*-Co4PyP-800 it is understood that the N peak corresponds to pyridinic (398.6 eV), pyrrolic (400.4 eV) and pyridine-N-oxide (402.1 eV). However, in the case of *p*-Co3PyP-800, there are only pyridinic (398.5 eV) and pyrrolic (400.2 eV) N peaks [24,51].

Deconvoluted spectrum of *p*-Co4PyP-800 indicated the presence of metallic cobalt in the pyrolysed sample (779.7 eV) which is absent in the same of unpyrolysed one, *p*-Co4PyP. This is an indication on the formation of cobalt nanoparticle on pyrolysis. The other peaks in the pyrolysed samples are at 781.2 eV (cobalt oxides), 785.5 eV (minor pyrolysed byproducts $Co(CO)_4$) and 795.9 eV ($Co2P_{1/2}$) as in the case of pyrolysed CoTPP [52]. Similar peak positions are seen for *p*-Co3PyP-800 also. The peak at 779.2 eV corresponds to the metallic cobalt present in the pyrolysed sample, 780.4 eV to cobalt oxides, 784.8 eV to $Co(CO)_4$ and 795.3 eV to Co $2P_{1/2}$.

There is a broad peak in the C 1 s region of XPS of *p*-Co4PyP-800. This peak is assigned to C–C (284.7 eV), C–O (286.3 eV) and N–C=O (288.3 eV) after deconvolution [50]. Similar behaviour is observed in the case of *p*-Co3PyP-800 (284.7 eV, 286.3 eV and 288.6 eV, respectively). The presence of oxygen can be ascribed to atmospheric O_2, CO_2 and H_2O that are adsorbed onto the surface of the samples as well as from the acetate ions which may be present as the counter ions for the cobalt present at the periphery of the porphyrins (cobalt ions to which the *meso*-pyridyl groups are interacting as ligands) [49,52].

3.2.5. BET surface area analysis

N_2-adsorption and desorption isotherms of *p*-Co4PyP-800 exhibited type-IV isotherm [24,52] (Fig. 9a). This indicates that it is a mesoporous material. Specific surface area of *p*-Co4PyP-800 (~109 m^2g^{-1}) is higher than that of *p*-Co4PyP (~11.552 m^2g^{-1}). The average pore size are 8.88 nm and 9.70 nm for *p*-Co4PyP and *p*-Co4PyP-800, respectively. This shows that pyrolysis at 800 °C, the pore sizes of the *p*-Co4PyP have increased, which is ascribed to the shrinkage of the pore walls at higher temperatures (Fig. 9b,

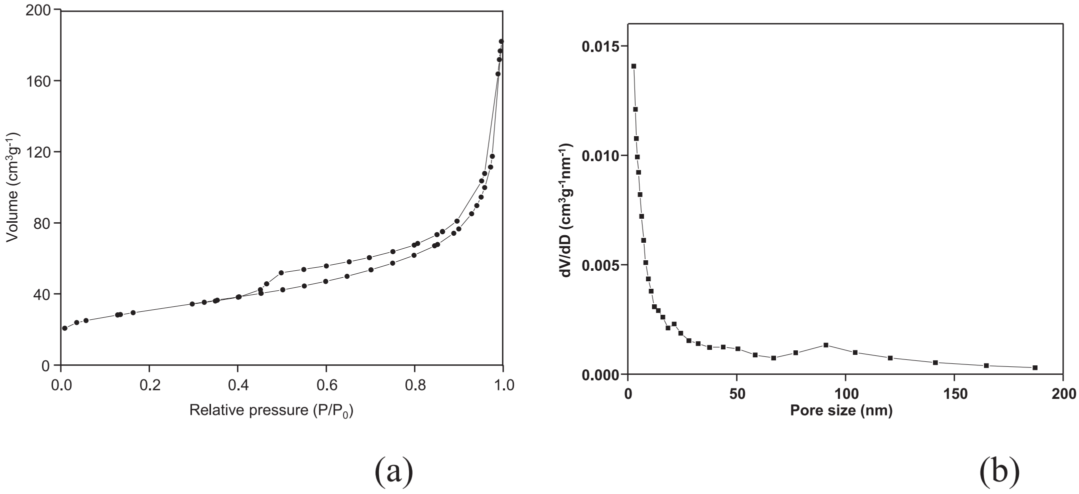

(a)

(b)

Fig. 9. (a) Adsorption-desorption curve and (b) BJH plot of *p*-Co4PyP-800.

Table 2
Surface area analysis parameters.

Sample	Surface area(m^2g^{-1})	Mesopore size(nm)	Pore volume(cm^3g^{-1})
p-Co4PyP	11.552	8.878	0.0562
p-Co4PyP-800	108.87	9.699	0.3823

Table 3
Catalytic parameters of ORR.

Samples	Electron transfer at −0.45V	Onset Potential (V)	Maximum Current (mA/cm^2)
p-Co4PyP	1.6	−0.214	2.5
p-Co4PyP-400	1.9	−0.200	2.7
p-Co4PyP-600	1.7	−0.140	2.3
p-Co4PyP-800	2.313	−0.100	7.0
p-Co3PyP	1.79	−0.300	1.1
p-Co3PyP-400	1.47	−0.270	1.4
p-Co3PyP-600	1.41	−0.190	2.0
p-Co3PyP-800	2.11	−0.120	4.3
Co3PyP-800–4 hrs	1.007	-0.300	2.3
Co3PyP-800–24hrs	1.72	0.370	1.75

Table 2). The higher surface area and the pore size of *p*-Co4PyP-800 can be attributed to the carbonization followed by structural rearrangement of *p*-Co4PyP framework on heating. *p*-Co4PyP has narrow pore-size distribution. The transportation of O_2 to the catalytically active sites is supported by the large-pore structures. High surface area helps in the better interaction of O_2 with the active centre [50,53].

3.3. Oxygen reduction reaction (ORR)

ORR was carried out using pyrolysed samples as the modifying agents (electrocatalyst for ORR) for GCE in alkaline medium (0.1 M KOH). The catalytic parameters for the ORR are summarized in Table 3. *p*-Co4PyP-800 displayed a more positive onset potential (−0.10 V) than that of *p*-Co4PyP-600 (−0.14 V), *p*-Co4PyP-400 (−0.2 V) and *p*-Co4PyP (−0.21 V) during ORR (Fig. 10a). *p*-Co4PyP-800 showed a highly stable diffusion-limiting current (7.0 mAcm^{-2}). On the basis of the RDE currents, the electron transfer number (n) of *p*-Co4PyP-800 is found to be 2.313 at −0.45 V suggesting two-electron oxygen reduction process (Fig. 10c and e). *p*-Co4PyP-600, *p*-Co4PyP-400 and *p*-Co4PyP, exhibited relatively lower n values 1.7, 1.9 and 1.6, respectively, at −0.45 V.

Similarly, ORR was carried out using samples of *p*-Co3PyP pyrolysed at different temperatures. *p*-Co3PyP-800 displayed a more positive onset potential (−0.12 V) than that of *p*-Co3PyP-600 (−0.19 V), *p*-Co3PyP-400 (−0.27 V) and *p*-Co3PyP (−0.30 V) (Fig. 10b). The diffusion-limiting current showed by *p*-Co3PyP-800 is 4.35 mAcm^{-2} which is superior to that of *p*-Co3PyP, *p*-Co3PyP-400 and *p*-Co3PyP-600. The electron transfer number (n) of *p*-Co3PyP-800 was calculated to be 2.113 at −0.45 V (Fig. 10d and f) which is slightly lower than that of *p*-Co4PyP-800. Other pyrolysed samples of *p*-Co3PyP also showed relatively lesser value compared to the 4-pyridyl counterparts.

On comparing the data (Fig. 11), it is observed that *p*-Co4PyP is relatively a better electrocatalyst than *p*-Co3PyP under all pyrolysed conditions (both in terms of current and potential). There might be a slight excess of Co nanoparticle formed on pyrolysing *p*-Co4PyP which in turn has resulted due to the favourable coordination geometry of the 4-pyridyl group at the *meso* position of the porphyrin in binding to the cobalt ion during the metalation reaction. The supramolecular conformational aspects of *meso*(3- and 4- pyridyl) isomers of tetraruthenated porphyrins on the electrocatalytic activities have been reported [54]. Metallic nanoparticle, especially, cobalt nanoparticles are known to be active for the reduction of dioxygen [55]. The carbonaceous material formed from the porphyrinic macrocycles on pyrolysis of the coordination polymer acts as the matrix for the otherwise unstable cobalt nanoparticle and help in its ORR activity. The presence of cobalt oxides also might have played a role in the ORR activity. However, as reported in the oxygen reduction activity of Co4PyP synthesized using DMF

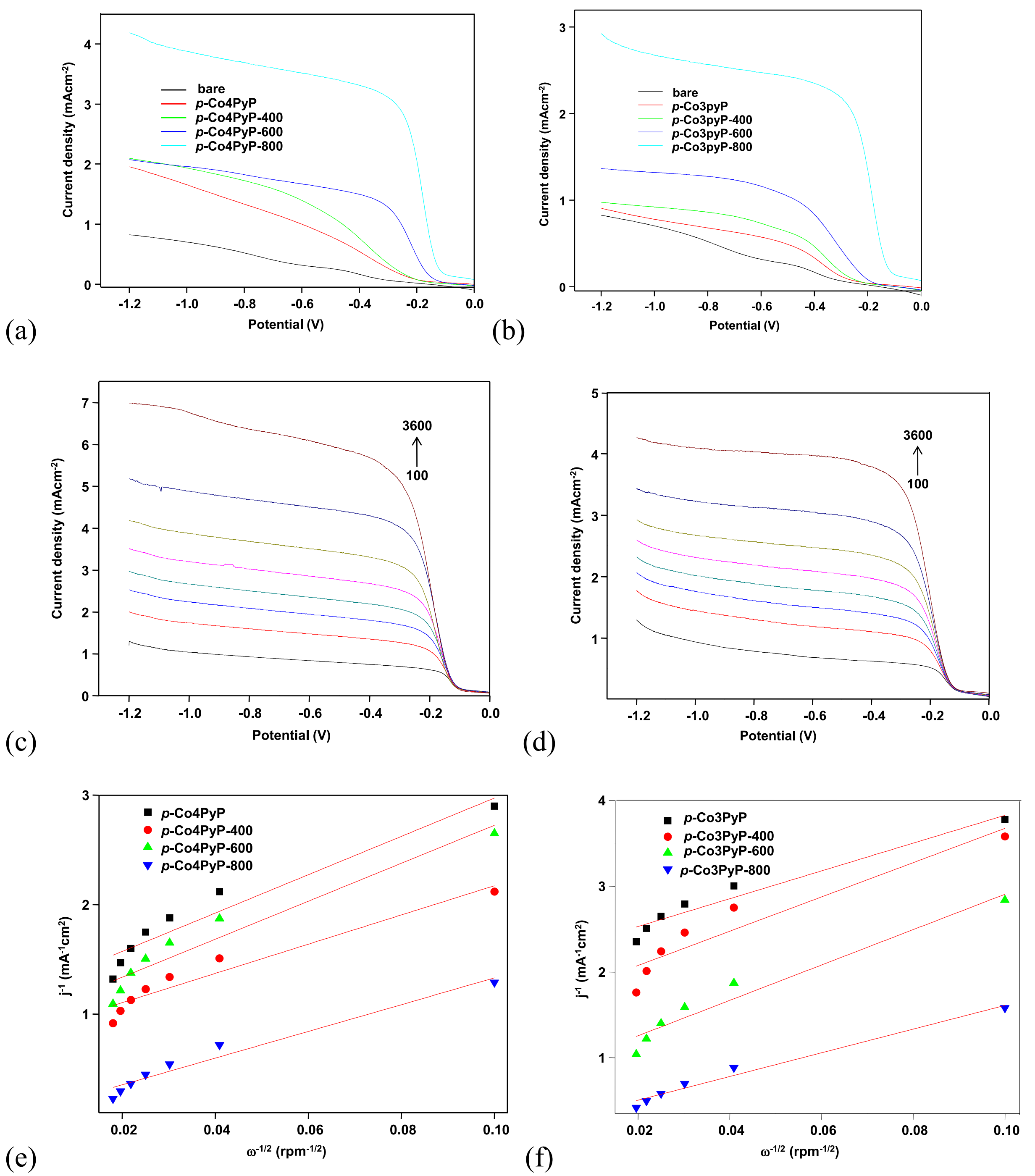

Fig. 10. LSV curves (2600 rpm) of different samples (a,b), RDE polarization curve of *p*-Co4PyP-800 and *p*-Co3PyP-800 at different rotation rates from 100 to 3600 in O_2-saturated 0.1 M KOH solution (c,d) and Koutecky-Levich plot of different samples of *p*-Co4PyP and *p*-Co3PyP at −0.45 V (e,f).

as the solvent [24], the activity cannot be due to the CoN_4 centre as no peak corresponding to Co-N bond is seen in the XPS investigation.

Co3PyP prepared using DMF as the solvent [16] has also been investigated for ORR after pyrolysing at 800 °C (Fig. 12, Table 3) for the comparison of its activity towards ORR. For this, we have carried out metalation reactions in DMF for two different refluxing durations. In the first case, the refluxing of the reaction mixture was carried out for 4 h (for comparison with our reaction condition) and in the second case the refluxing period was extended to 24 h (as reported). Both the samples were pyrolysed at 800 °C and named accordingly (Co3PyP-800–4 hrs and Co3PyP-800–24 hrs). For *p*-Co3PyP-800 (the present work), the n factor is 2.113 as mentioned above where as for Co3PyP-800–4 hrs and Co3PyP-800–24 hrs it is, respectively, 1.007 and 1.72 at −0.45 V (Figure S2). It is clear from the figure that samples in which DMF is used for the metalation, there is no considerable amount of current at −0.12 V which is the onset potential of *p*-Co3PyP-800 in ORR. This difference in the n factor as well as in the amount of current also gives an indication on the increased amount of Co content resulted during the synthesis (leading to the formation of coordination polymer) on using $CHCl_3$–CH_3OH as the solvent system in the present work.

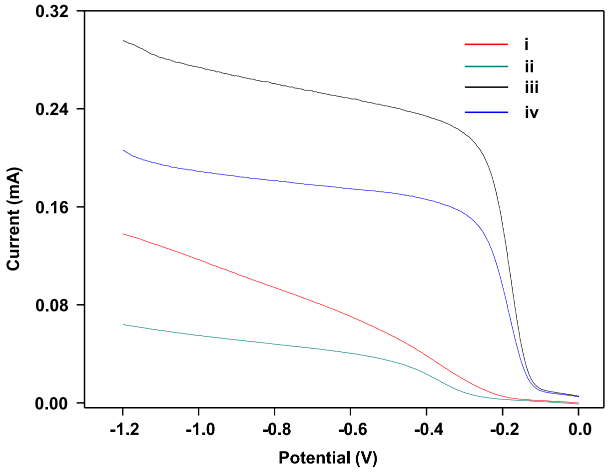

Fig. 11. (i) *p*-Co4PyP and (ii) *p*-Co3PyP before pyrolysis under oxygen atmosphere; (iii) *p*-Co4PyP and (iv) *p*-Co3PyP under pyrolysis at 800 °C under oxygen atmosphere (all in 0.1 M KOH, 2600 rpm).

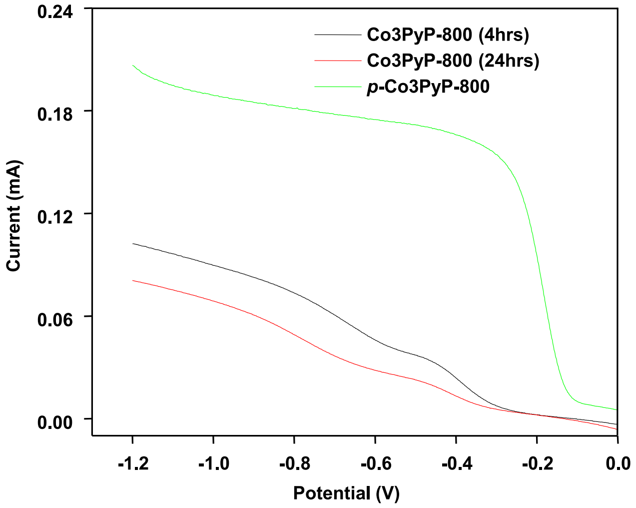

Fig. 12. LSV curves (2600 rpm) of different samples in O_2 saturated 0.1 M KOH solution.

4. Conclusion

In this work, the possibility of peripheral coordination of pyridylporphyrins with metal ion is investigated by treating isomers of pyridylporphyrins with cobalt metal ion carrier in different ratios. This study has shed light on the positional aspects of heteroatom in deciding the yield of the reaction. We have tried to metalate the isomeric pyridylporphyrins in simple solvent system, $CHCl_3$–CH_3OH and have observed different solubility characteristics for the product from what is reported when DMF was used as the solvent for the same. This difference is attributed to the difference in the extent of peripheral coordination of the molecule in this solvent system leading to the formation of coordination polymer. The coordination polymers of 3- and 4- pyridylporphyrins under pyrolysed (at 800 °C) conditions acts as electrocatalysts for the oxygen reduction through 2-electron pathway forming H_2O_2 in alkaline medium at onset potentials −0.12 V and – 0.10 V, respectively. The increased activity of these porphyrins compared to the unpyrolysed samples is attributed to the formation of cobalt nanoparticle and cobalt oxides on pyrolysis. Formation of coordination polymer helps in increasing the cobalt content in the pyrolysed samples.

Declaration of Competing Interest

The authors declare that they have no known competing financial interests or personal relationships that could have appeared to influence the work reported in this paper.

CRediT authorship contribution statement

Neha Saran: Methodology, Validation, Investigation. **Tincy Lis Thomas:** Methodology, Resources. **Purushothaman Bhavana:** Conceptualization, Methodology, Supervision, Writing - review & editing.

Acknowledgements

PB gratefully acknowledges Science & Engineering Research Board (SERB), India for the research grant (EMR/2016/002367). Dr. Richa Singhal and Ms. Ishita of Department of Chemical Engineering, BITS, Pilani – K K Birla Goa campus is gratefully acknowledged for their help in pyrolysing samples.

Supplementary materials

Supplementary material associated with this article can be found, in the online version, at doi:10.1016/j.molstruc.2021.130032.

References

[1] L. Cook, G. Brewer, W. Wong-Ng, Structural aspects of porphyrins for functional materials applications, Crystals 7 (2017) 223, doi:10.3390/cryst7070223.
[2] Y. Inada, Y. Nakano, M. Inamo, M. Nomura, S. Funahashi, Structural characterization and formation mechanism of sitting-atop (SAT) complexes of 5,10,15,20-tetraphenylporphyrin with divalent metal ions. Structure of the Cu(II)-SAT complex as determined by fluorescent extended X-ray absorption fine structure, Inorg. Chem. 39 (2000) 4793–4801.
[3] Z.-Y. Zou, X-M.Wang Ping-Ding, Z.-Q. Liang, X.-T. Tao, Sandwich-type porphyrin complexes as efficient sensitizers for triplet-triplet annihilation upconversion, ChemistrySelect 5 (2020) 1713–1717.
[4] D. Furutsu, A. Satake, Y. Kobuke, A giant supramolecular light-harvesting antenna−acceptor composite, Inorg. Chem. 44 (2005) 4460–4462.
[5] S. Lipstman, I. Goldberg, Versatile supramolecular reactivity of zinc-tetra(4-pyridyl)porphyrin in crystalline solids: polymeric grids with zinc dichloride and hydrogen-bonded networks with mellitic acid, Beilstein J. Org. Chem. 5 (2009), doi:10.3762/bjoc.5.77.
[6] E.B. Fleischer, The structure of porphyrins and metalloporphyrins, Acc. Chem. Res 3 (1970) 105–112.
[7] A. Ghosh, S.M. Mobin, R. Fröhlich, R.J. Butcher, D.K. Maity, M. Ravikanth, Effect of five membered versus six membered meso-substituents on structure and electronic properties of Mg(II) porphyrins: a combined experimental and theoretical study, Inorg. Chem. 49 (2010) 8287–8297.
[8] I. Goldberg, Design strategies for supramolecular porphyrin-based materials, CrystEngComm 4 (2002) 109–116.
[9] P. Muthukumar, S.A. John, Highly sensitive detection of HCl gas using a thin film of meso-tetra(4-pyridyl)porphyrin coated glass slide by optochemical method, Sens. Actuators B **Chem.** 159 (2011) 238–244.
[10] P. Guo, G. Zhao, P. Chen, B. Lei, L. Jiang, H. Zhang, W. Hu, M. Liu, Porphyrin nanoassemblies via surfactant-assisted assembly and single nanofiber nanoelectronic sensors for high-performance H_2O_2 vapor sensing, ACS Nano 8 (2014) 3402–3411.
[11] L. Zhao, M. Li, M. Liu, Y. Zhang, C. Wu, Y. Zhang, Porphyrin-functionalized porous polysulfone membrane towards an optical sensor membrane for sorption and detection of cadmium(II), J. Hazard. Mater. 301 (2016) 233–241.
[12] K. Berijani, H. Hosseini-Monfared, Aerobic enantioselective epoxidation of olefins mediated by an easy-to-prepare recyclable manganese-porphyrin, Mol. Catal. 433 (2017) 136–144.
[13] J.S. Rebouças, M.E.M.D. de Carvalho, Y.M. Idemori, Perhalogenated 2-pyridylporphyrin complexes: synthesis, self-coordinating aggregation properties, and catalytic studies, J. Porphyrins Phthalocyanines 6 (2002) 50–57.
[14] Z. Zhang, X. Li, Q. Zhao, J. Ke, Y. Shi, P. Ndokoye, L. Wang, Facile synthesis and characterizations of copper–zinc-10,15,20-tetra(4-pyridyl) porphyrin (Cu–ZnT-PyP) coordination polymer with hexagonal micro-lump and micro-prism morphologies, J. Colloid Interface Sci. 432 (2014) 229–235.

[15] Y. Li, J. Xiao, T.E. Shubina, M. Chen, Z. Shi, M. Schmid, H.-P. Steinrück, J.M. Gottfried, N. Lin, Coordination and metalation bifunctionality of Cu with 5,10,15,20-tetra(4-pyridyl)porphyrin: toward a mixed-valence two-dimensional coordination network, J. Am. Chem. Soc 134 (2012) 6401–6408.
[16] S. Lipstman, I. Goldberg, Supramolecular crystal chemistry of tetra(3-pyridyl)porphyrin. 2. Two- and three-dimensional coordination networks with cobalt and cadmium ions, Cryst. Growth Des. 10 (2010) 5001–5006.
[17] N. Shi, L. Xie, H. Sun, J. Duan, G. Yin, Z. Xu, W. Huang, Facile synthesis of shape and size tunable porphyrinoid coordination polymers: from copper porphyrin nanoplates to microspindles, Chem. Commun. 47 (2011) 5055–5057.
[18] W. Sun, H. Wang, D. Qi, L. Wang, K. Wang, J. Kan, W. Li, Y. Chen, J. Jiang, 5,10,15,20-tetra(4-pyridyl)porphyrinato zinc coordination polymeric particles with different shapes and luminescent properties, CrystEngComm 14 (2012) 7780–7786.
[19] P.H. Kumar, S. Prashanthi, P.R. Bangal, Role of hydrogen bonding in the photophysical properties of isomeric tetrapyridylporphyrins in aprotic solvent, J. Phys. Chem. A 115 (2011) 631–642.
[20] Y. Diskin-Posner, G.K. Patra, I. Goldberg, Supramolecular porphyrin-based materials. Assembly modes of [5,10,15,20-tetrakis(4-hydroxyphenyl)porphyrinato]zinc with bipyridyl ligands, CrystEngComm 4 (2002) 296–301.
[21] C.M. Drain, F. Nifiatis, A. Vasenko, J.D. Batteas, Porphyrin tessellation by design: metal-mediated self-assembly of large arrays and tapes, Angew. Chem. Int. Ed. 37 (1998) 2344–2347.
[22] R.J.H. Chan, Y.O. Su, T. Kuwana, Electrocatalysis of oxygen reduction. 5. Oxygen to hydrogen peroxide conversion by cobalt(I1) tetrakis(N-methyl-4-pyridy1)porphyrin, Inorg. Chem. 24 (1985) 3777–3784.
[23] L. Jiang, L. Cui, X. He, Cobalt-porphyrin noncovalently functionalized graphene as nonprecious-metal electrocatalyst for oxygen reduction reaction in an alkaline medium, J. Solid State Electrochem. DOI 10.1007/s10008-014-2628-3.
[24] C. Li, Z. Han, Y. Yu, Y. Zhang, B. Dong, A. Kong, Y. Shan, Efficient oxygen electroreduction over ordered mesoporous Co–N-doped carbon derived from cobalt porphyrin, RSC Adv. 6 (2016) 15167–15174.
[25] K. Shigehara, F.C. Anson, Electrocatalytic activity of three iron porphyrins in the reductions of dioxygen and hydrogen peroxide at graphite electrodes, J. Phys. Chem. 86 (1982) 2776–2783.
[26] P.T. Smith, Y. Kim, B.P. Benke, K. Kim, C.J. Chang, Supramolecular tuning enables selective oxygen reduction catalyzed by cobalt porphyrins for direct electrosynthesis of hydrogen peroxide, Angew. Chem. Int. Ed. 59 (2020) 4902–4907.
[27] S. Dey, B. Mondal, S. Chatterjee, A. Rana, S. Amanullah, A. Dey, Molecular electrocatalysts for the oxygen reduction reaction, Nat. Rev. Chem. 1 (2017), doi:10.1038/s41570-017-0098.
[28] A. Morozan, S. Campidelli, A. Filoramo, B. Jousselme, S. Palacin, Catalytic activity of cobalt and iron phthalocyanines or porphyrins supported on different carbon nanotubes towards oxygen reduction reaction, Carbon 49 (2011) 4839–4847.
[29] P.K. Sonkar, K. Prakash, M. Yadav, V. Ganesan, M. Sankar, R. Gupta, D.K. Yadav, Co(II)-porphyrin-decorated carbon nanotubes as catalysts for oxygen reduction reactions: an approach for fuel cell improvement, J. Mater. Chem. A 5 (2017) 6263–6276.
[30] W.S. Cardoso, M.S.P. Francisco, R. Landers, Y. Gushikema, Co (II) porphyrin adsorbed on SiO2/SnO2/phosphate prepared by the sol–gel method application in electroreduction of dissolved dioxygen, Electrochim. Acta 50 (2005) 4378–4384.
[31] F.C. Anson, C.-L. Ni, J.-M. Saveant, Electrocatalysis at redox polymer electrodes with separation of the catalytic and charge propagation roles. Reduction of O_2 to H_2O_2 as catalyzed by cobalt(I1) tetrakis(4-N-methylpyridy1)porphyrin, J. Am. Chem. Soc. 107 (1985) 3442–3450.
[32] B.D. Matson, C.T. Carver, A.V. Ruden, J.Y. Yang, S. Raugei, J.M. Mayer, Distant protonated pyridine groups in water-soluble iron porphyrin electrocatalysts promote selective oxygen reduction to water, Chem. Commun. 48 (2012) 11100–11102.
[33] F. D'Souza, R.G. Deviprasad, Y.-Y. Hsieh, Synthesis and studies on the electrocatalytic reduction of molecular oxygen by non-planar cobalt (II) tetrakis-N-methyl pyridyl)-β-octabromoporphyrin, J. Electroanal. Chem. 411 (1996) 167–171.
[34] P.A. Forshey, T. Kuwana, Electrochemistry of Oxygen Reduction. 4. Oxygen to water conversion by iron(I1) tetrakis(N-methyl-4-pyridy1)porphyrin via hydrogen peroxide, Inorg. Chem. 22 (1983) 699–707.
[35] A. Bettelheim, T. Kuwana, Rotating-ring-disc analysis of iron tetra(N-methylpyridyl)porphyrin in electrocatalysis of oxygen, Anal. Chem. 51 (1979) 2257–2260.
[36] T. Okada, M. Gokito, M. Yuasa, I. Sekine, Oxygen reduction characteristics of heat-treated catalysts based on cobalt-porphyrin ion complexes, J. Electrochem. Soc. 145 (1998) 815–822.
[37] S. Dong, Q. Qiu, Electrodeposition of platinum particles on glassy carbon modified with cobalt porphyrin and nafion film and their electrocatalytic reduction of dioxygen, J. Electroanal. Chem. 314 (1991) 223–239.
[38] F. D'Souza, Y.-Y. Hsieh, G.R. Deviprasad, Four-electron electrocatalytic reduction of dioxygen to water by an ion-pair cobalt porphyrin dimer adsorbed on a glassy carbon electrode, Chem. Commun. (1998) 1027–1028.
[39] S. Popovici, W. Leyffer, R. Holze, On the mechanism of dioxygen electroreduction at transition metal meso-tetrakis pyridyl porphyrins—a comparative spectroelectrochemical study, J. Porphyrins Phthalocyanines 3 (1999) 265–282.
[40] C. Shi, F.C. Anson, Electrocatalysis of the reduction of O_2 to H_2O by tetraruthenated cobalt meso tetrakis(4-pyridy1)porphyrin adsorbed on graphite electrodes, Inorg. Chem. 31 (1992) 5078–5083.
[41] S.-Q. Liu, J.-Q. Xu, H.-R. Sun, D-M. Li, meso-Tetrakis(4-N-benzylpyridyl)porphyrin and its supramolecular complexes formed with anionic metal–oxo cluster: spectroscopy and electrocatalytic reduction of dioxygen, Inorganica Chim. Acta 306 (2000) 87–93.
[42] A. Bettelheim, R.J.H. Chan, T. Kuwana, Electrocatalysis of oxygen reduction Part II. Adsorbed cobalt(III) tetrapyridylporphyrin on glassy carbon electrode, J. Electroanal. Chem. 99 (1979) 391–397.
[43] M.L. Rigsby, D.J. Wasylenko, M.L. Pegis, J.M. Mayer, Medium effects are as important as catalyst design for selectivity in electrocatalytic oxygen reduction by iron−porphyrin complexes, J. Am. Chem. Soc. 137 (2015) 4296–4299.
[44] S. Vengatesan, E. Cho, I.-H. Oh, Development of non-precious oxygen reduction reaction catalyst for polymer electrolyte membrane fuel cells based on substituted cobalt porphyrins, Korean J. Chem. Eng. 29 (2012) 621–626.
[45] A.D. Adler, F.R. Longo, J.D. Finarelli, J. Goldmacher, J. Assour, L. Korsakoff, A simplified synthesis for meso-tetraphenylporphin, J. Org. Chem. 32 (1967) 476.
[46] F. Shigenobu, S. Keiji, T. Motoharu, Kinetics and mechanism of cobalt(ii) incorporation into meso-tetra(4-pyridyl)porphine in acetic acid, Bull. Chem. Soc. Jpn. 54 (1981) 2695–2699.
[47] J.-M. You, H.S. Han, H.K. Lee, S. Cho, S. Jeon, Enhanced electrocatalytic activity of oxygen reduction by cobalt-porphyrin functionalized with graphene oxide in an alkaline solution, Int. J. Hydrog. Energy 39 (2014) 4803–4811.
[48] A. Widelov, R. Larsson, ESCA and electrochemical studies on pyrolysed iron and cobalt tetraphenylporphyrins, Electrochim. Acta 37 (1992) 187–197.
[49] Z.-S. Wu, L. Chen, J. Liu, K. Parvez, H. Liang, J. Shu, H. Sachdev, R. Graf, X. Feng, K. Müllen, High-performance electrocatalysts for oxygen reduction derived from cobalt porphyrin-based conjugated mesoporous polymers, Adv. Mater. 26 (2014) 1450–1455.
[50] Z. Sun, J. Li, H. Zheng, X. Liu, S. Ye, P. Du, Pyrolyzed cobalt porphyrin-modified carbon nanomaterial as an active catalyst for electrocatalytic water oxidation, Int. J. Hydrog. Energy 40 (2015) 6538–6545.
[51] S. Pylypenko, S. Mukherjee, T.S. Olson, P. Atanassov, Non-platinum oxygen reduction electrocatalysts based on pyrolyzed transition metal macrocycles, Electrochim. Acta 53 (2008) 7875–7883.
[52] K. Artyushkova, S. Levendosky, P. Atanassov, J. Fulghum, XPS structural studies of nano-composite non-platinum electrocatalysts for polymer electrolyte fuel cells, Top. Catal. 46 (2007) 263–275.
[53] D. Liu, Y.-T. Long, Superior catalytic activity of electrochemically reduced graphene oxide supported iron phthalocyanines toward oxygen reduction reaction, ACS Appl. Mater. Interfaces 7 (2015) 24063–24068 2015.
[54] I. Mayer, M.N. Eberlin, D.M. Tomazela, H.E. Toma, K. Araki, Supramolecular conformational effects in the electrocatalytic properties of electrostatic assembled films of meso(3- and 4-pyridyl) isomers of tetraruthenated porphyrins, J. Braz. Chem. Soc. 16 (2005) 418–425.
[55] Z-s Yin, T-h Hu, J-l Wang, C. Wang, Z-x Liu, J-w Guo, Preparation of highly active and stable polyaniline-cobalt-carbon nanotube electrocatalyst for oxygen reduction reaction in polymer electrolyte membrane fuel cell, Electrochim. Acta 119 (2014) 144–154.